Skeletal development is regulated by fibroblast growth factor receptor 1 signalling dynamics

Mohammad K. Hajihosseini[1,*,‡], Maria D. Lalioti[1,†,‡], Sandrine Arthaud[1], Helen R. Burgar[1], Jill M. Brown[2], Stephen R. F. Twigg[2], Andrew O. M. Wilkie[2] and John K. Heath[1,§]

[1]School of Biosciences, University of Birmingham, Edgbaston, Birmingham B15 2TT, UK
[2]Weatherall Institute of Molecular Medicine, The John Radcliffe Hospital, Headington, Oxford OX3 9DS, UK
*Present address: School of Biological Sciences, University of East Anglia, Norwich NR4 7TJ, UK
†Present address: Yale School of Medicine; BCMM 147, 295 Congress Avenue CT 06511 New Haven, USA
‡These authors contributed equally to this work
§Author for correspondence (e-mail: j.k.heath@bham.ac.uk)

Accepted 14 October 2003

Development 131, 325-335
Published by The Company of Biologists 2004
doi:10.1242/dev.00940

Summary

Ligand-dependent signalling pathways have been characterised as having morphogen properties where there is a quantitative relationship between receptor activation and response, or threshold characteristics in which there is a binary switch in response at a fixed level of receptor activation. Here we report the use of a bacterial artificial chromosome (BAC)-based transgenic system in which a hypermorphic mutation has been introduced into the murine *Fgfr1* gene. These mice exhibit cranial suture and sternal fusions that are exacerbated when the BAC copy number is increased. Surprisingly, increasing mutant BAC copy number also leads to the de novo appearance of digit I polydactyly in the hind limb and transformations of the vertebrae. Polydactyly is accompanied by a reduction of programmed cell death in the developing hind limb. Candidate gene analysis reveals downregulation of *Dkk1* in the digit I field and upregulation of *Wnt5a* and *Hoxd13*. These findings show that Fgfr1-mediated developmental pathways exhibit differing signalling dynamics, whereby development of the cranial sutures and sternum follows a morphogen mode, whereas development of the vertebral column and the hind limbs has threshold signalling properties.

Supplemental data available online

Key words: Fgf, Signalling, Skeleton

Introduction

Although much is known about the connectivity of receptor-mediated developmental signalling pathways, relatively little is known about the relationship between the dynamics of receptor activation and the ensuing response. Freeman and Gurdon have drawn a distinction between 'morphogen signalling' – in which the response is quantitatively linked to the concentration of activating ligand (and therefore activated receptors) – and 'threshold' signalling in which the response is triggered in a binary manner at a pre-set level of receptor activation (Freeman and Gurdon, 2002). In both cases the critical value in determining the outcome is the degree of receptor activation. In order to characterise receptor-controlled developmental pathways as having morphogen or threshold characteristics, it is necessary to quantitatively manipulate receptor signalling dynamics in a controlled fashion and observe the developmental outcome. A particular opportunity to examine this issue is in the fibroblast growth factor receptor (Fgfr) system (reviewed by Johnson and Williams, 1993; Ornitz and Itoh, 2001), where it has been shown that specific hypermorphic mutations in the extracellular ligand recognition domain of Fgfrs 1 and 2 exhibit quantitatively distinct affinities for Fgf ligands, compared with their wild-type counterparts (Anderson et al., 1998). This relationship can be exploited to probe the developmental significance of Fgfr signalling dynamics in vivo. Here we show, by incrementally manipulating the ratio of mutant to wild-type receptors, that Fgfr1 signalling pathways exhibit 'morphogen' signalling characteristics in the development of the skull, and a cryptic 'threshold' property in the development of the limbs and axial skeleton.

Specific hypermorphic mutations in Fgfr1 and Fgfr2 are the cause of seven clinically distinct craniosynostosis syndromes (Passos-Bueno et al., 1999), the phenotypic hallmark of which is the obliteration of sutures separating calvarial bones (reviewed by Wilkie and Morriss-Kay, 2001; Ornitz and Marie, 2002). Craniosynostosis is, in particular syndromes, accompanied by limb defects ranging in severity from a broadening of the thumbs and great toes in Pfeiffer syndrome, to boney and soft tissue syndactyly of the digits in Apert syndrome. The extent and severity of phenotypes correlates with the type and position of the mutations, and with the Fgfr gene involved. Apert syndrome (which exhibits strong limb and skull defects) generally involves specific missense substitutions in two adjacent residues of Fgfr2: Ser252Trp and Pro253Arg. These both lie in the 'linker' region joining Ig-like domains II and III (Oldridge et al., 1997; Ibrahimi et al., 2001). The phenotypically milder Pfeiffer syndrome arises from a missense substitution in Fgfr1 – Pro252Arg – in the topologically equivalent 'linker' residue to Fgfr2 Pro253Arg.

Fgfr2 'linker' mutations have been shown to exhibit increased affinities for specific Fgf ligands (Anderson et al., 1998; Ibrahimi et al., 2001) because of the additional receptor/ligand contact site introduced by the missense substitution. This finding suggests that Apert/ Pfeiffer-type linker domain substitutions result in receptors that are activated at lower concentrations of ligand compared with their wild-type counterparts, and that exhibit quantitatively distinct ligand-dependant signalling dynamics. As receptor activation is initiated by ligand-mediated receptor dimerisation (reviewed by Schlessinger, 2000), only mutant receptor homodimers exhibit mutant signalling dynamics. This consideration predicts that the phenotypic consequences of mutant receptor signalling will be dictated by the ratio of mutant to wild-type receptors, as elevating the ratio will favour the formation of mutant homodimer complexes in the presence of appropriate ligands. Thus, varying the expression of mutant receptors provides a means to study the consequences of quantitative changes in Fgfr signalling dynamics.

Here we employ a novel bacterial artificial chromosome (BAC)-based transgenic system (Lalioti and Heath, 2001) to dissect the molecular consequences of mutant Fgfr action in vivo. We have introduced into the mouse germ line a BAC encoding the entire mouse *Fgfr1* gene that harbours a single nucleotide substitution corresponding to the human Pfeiffer syndrome mutation Pro252Arg (Muenke et al., 1994). We find that, in contrast to BACs harbouring silent single nucleotide substitutions, the presence of the mutant BAC transgene yields skeletal defects that involve both membranous and endochondral modes of ossification, resembling those seen in human Pfeiffer patients. Doubling the BAC gene copy number – thereby incrementally elevating signalling through mutant receptors – yields an increase in the severity of the ossification defects, and an unexpected de novo appearance of pre-axial polydactyly of the hindlimbs and homeotic transformation of the vertebrae. These findings demonstrate the existence of a Fgfr1 signalling threshold governing the development of digit I and vertebral patterning. This study also shows – as predicted by Freeman and Gurdon (Freeman and Gurdon, 2002) – that a single signalling pathway can exhibit both morphogen and threshold signalling properties depending on the level of receptor activation.

Materials and methods

Isolation and characterisation of a *Fgfr1* BAC clone

A mouse library [RPC-22 filters, from BacPac Resources (Osoegawa et al., 2000)] was probed with a digoxigenin-labelled *Fgfr1* cDNA, generated by PCR using primer sets: exon 1 (1L), 5′-GTGGAATATCCATGGAGGTAC-3′; and (2R), 5′-CTCCTCCGA-GGAGGAGTCATC-3′. Positive clones (HGMP, Hinxton, UK) were then screened by three PCR reactions, using sets of primers whose products would cover the entire 21 exons of the mouse *Fgfr1* gene. These primers were:

exon 1 (1L) and (3R), 5′-CCCAGAAGAGGAGGCACTTC-3′;

exon 7 (21L), 5′-AGATCTGGGAAGGGTCTAAG-3′ and (21R), 5′-CTCGAGTCTGGGAGCGAGAG-3′;

exon 19 (4L), 5′-ATACCGCTGGACCAGTACTC-3′ and (1R), 5′-TCAGCGCCGTTTGAGTCCACTG-3′.

Mutant *Fgfr1* fragments were generated by overlap PCR. Essentially, two complementary primers covering the region to be mutated were used in conjuction with a pair of external primers to produce two overlapping fragments using Pfu polymerase (Promega). The two fragments were then joined together in a second reaction using only the external primers. For the Pro252Arg mutation (BAC16) the complementary primer pairs were (16L) 5′-GAACGATCCCGGCACCGAC-3′, and external primers were (21L) and (21R) (see above). These products were then cloned into the *Bam*HI-*Sal*I sites of the pKOV-kan shuttle vector in preparation for modification of the BAC as described previously (Lalioti and Heath, 2001).

Generation and screening of transgenic animals

Modified BACs were prepared for pronuclear injection as described (Chrast et al., 1999; Lalioti and Heath, 2001), and injected as linearized DNA (0.3-3 ng/μl) into fertilized oocytes. Genomic tail DNA from offspring was subjected to the following PCR conditions: 1 cycle of 5 minutes at 94°C; 10 cycles of 20 seconds at 94°C, 20 seconds at 60°C (with 1°C decrease per cycle), 30 seconds at 72°C; 20 cycles of 20 seconds at 94°C, 20 seconds at 50°C, 30 seconds at 72°C; 1 cycle of 5 minutes at 72°C. Primer pairs used were exon 7 (31L): 5′-TGACATGCCTGTCCTCTCTGTG-3′ and (34R) 5′-CCCTACTAGGAGATAGTATGTG-3′. The PCR products were then digested for 2 hours with *Msp*I (for BAC16) or *Pst*I (for BAC15), and resolved on 3% high resolution agarose gels (Elchrom Scientific).

To test expression of the transgene, 100 ng of total liver RNA isolated using Trizol® Reagent (GibcoBRL) was subjected to One Step RT-PCR (Qiagen) using the primers (8L) 5′-ACCTACC-AGCTTGACGTCGTG-3′ and (6R) 5′-CATTTCCTTGTCGG-TGGTATTAAC-3′, as per manufacturer recommendations.

Skeletal staining

Skeletons from embryos, new born or adult mice were stained with Alcian Blue and/or Alizarin Red as described by McLeod (McLeod, 1980). A full listing of the animals examined with phenotypic annotation is provided in supplementary Tables S1 and S2.

Analysis of BAC-transgene copy number and sites of integration by fluorescence in situ hybridisation (FISH)

FISH analysis was carried out as described by Buckle and Rack (Buckle and Rack, 1993). Essentially, chromosomes were isolated from splenic cells, previously cultured for 48 hours in the presence of lipopolysaccharide (Triman et al., 1975), and hybridised with a mixture containing a bitoin 16-UTP-labelled murine *Fgfr1* BAC probe and either Cy3-labelled mouse chromosome 8 paint or FITC-labelled mouse chromosome 4 paint (Cambio, Cambridge, UK). The hybridisation mixture contained 100 ng of biotinylated probe, 3 μg mouse COT-1 DNA (Invitrogen) and 20 μg salmon sperm DNA (Sigma), together with the appropriate amounts of paint, according to the manufacturer's instructions. The biotinylated *Fgfr1* probe was detected with either avidin Cy3.5 (Amersham Pharmacia) or avidin FITC (Vector Laboratories). Chromosomes were counterstained with 4′,6-diamidino-2-phenylindole (DAPI) at 1.5 μg/ml and analysed using an Olympus BX-60 microscope equipped with a Pinkel filter wheel. Images were captured and analysed using a SenSys cooled CCD camera (Photometrics, Tuscon), and MacProbe version 4.3 software (Applied Imaging, UK).

Quantitative PCR analysis of BAC copy number/ transgene expression

Genomic DNA was amplified with primers (31L) and (34R) (see above; the reverse oligonucleotide was fluorescently labelled) using the following cycling conditions: 1 cycle of 10 minutes at 94°C; then 25 cycles of 30 seconds at 94°C, 30 seconds at 58°C and 30 seconds at 72°C; followed by 10 minutes at 72°C. The PCR products were digested for 1 hour with *Msp*I and the fragments separated on an ABI 377 automated sequencer and analysed by GeneScan software (Applied Biosystems). cDNA (2 μl from a 40 μl first strand synthesis reverse transcription reaction using 2-5 μg total RNA) was amplified

with primers (8L) and (6R) (see above; the reverse oligonucleotide was fluorescently labelled), using the same cycling conditions as for genomic DNA except the annealing temperature was 55°C. PCR products were digested for 2 hours with *Msp*I and analysed as above.

Whole-mount in situ hybridisation (WMISH)

Whole embryos were isolated at appropriate stages of development from time-mated mice, counting noon of the day on which the vaginal plug was found as zero. Embryos were fixed overnight in 4% paraformaldehyde, dehydrated the following day through ascending concentrations of methanol/PBS containing 0.1% Tween-20, and stored until use in absolute methanol at –20°C. The genotype of each embryo (i.e. whether carrying low or high copies of the transgene) was verified by PCR (described above), using genomic DNA isolated from yolk sacs.

For WMISH, embryos were rehydrated in descending concentrations of methanol in PBS/Tween-20, treated with proteinase K, and hybridised at the appropriate temperatures (55-69°C) with sense (control) or anti-sense riboprobes generated from linearized plasmids containing the gene of interest (see Table S3 at http://dev.biologists.org/supplemental/). The protocol followed for WMISH was as previously described (Hajihosseini et al., 2001), with the exception that the colour development (NBT/BCIP) reaction was performed in the presence of polyvinyl alcohol (Sigma).

Detection of apoptotic cell by neutral red staining

Embryos were stained live as previously described (Hajihosseini and Heath, 2002). Briefly, soon after isolation, embryos were rinsed in freshly prepared 3% BSA/PBS and stained in the dark for 25 minutes (for E12.5) at room temperature in the same solution containing 0.05% Neutral Red. Excess dye was discarded and embryos were rinsed several times in 3% BSA/PBS, then in PBS and fixed for 15 minutess in 4% paraformaldehyde solution. Stained embryos were then photographed immediately.

Results

Generation and characterisation of BAC transgenic mice

A BAC construct harbouring a mutant *Fgfr1* allele (Pro252Arg, hereafter referred to as BAC16; Fig. 1A) was made as described in the Materials and methods, and by Lalioti and Heath (Lalioti and Heath, 2001). As a control, a similar construct harbouring a silent *Fgfr1* mutation (herein referred to as BAC15) was used. Transgenic lines were obtained by injection of the recombinant BAC DNA into fertilised eggs, with subsequent transfer of embryos to foster mothers. Founder mice carrying one or two copies of the transgenes (see below) were found to be viable and fertile, and were maintained on a C57-BL6 black background. Fluorescence in situ hybridisation (FISH) of splenic metaphase chromosomes derived from one particular line (designated BAC16/42) showed that the BAC transgene had integrated into the D3 region of chromosome 4 (Fig. 1B). The higher signal derived from the BAC transgene indicated that more than one copy had integrated. The results presented here are derived primarily from this line, although the phenotypes reported were seen in multiple independent lines. RT-PCR analysis on RNA isolated from mutant mice confirmed expression of the transgene in multiple tissues and showed this to be quantitatively comparable to the endogenous level of *Fgfr1* expression (Fig. 1C; and data not shown). Quantitative PCR of genomic DNA confirmed that the BAC16/42 allele had integrated two copies of the BAC (data not shown). When single integration site BAC16 mice were intercrossed to generate homozygous integration alleles, the copy number – as expected from integration of two tandem copies – doubled to 4 (Fig. 1B,D). Quantitative PCR on selected tissue RNAs revealed that the expression levels of the mutant *Fgfr1* gene were directly related to the BAC copy number and the endogenous wild-type gene copy number (data not shown). Examination of *Fgfr1* expression at selected

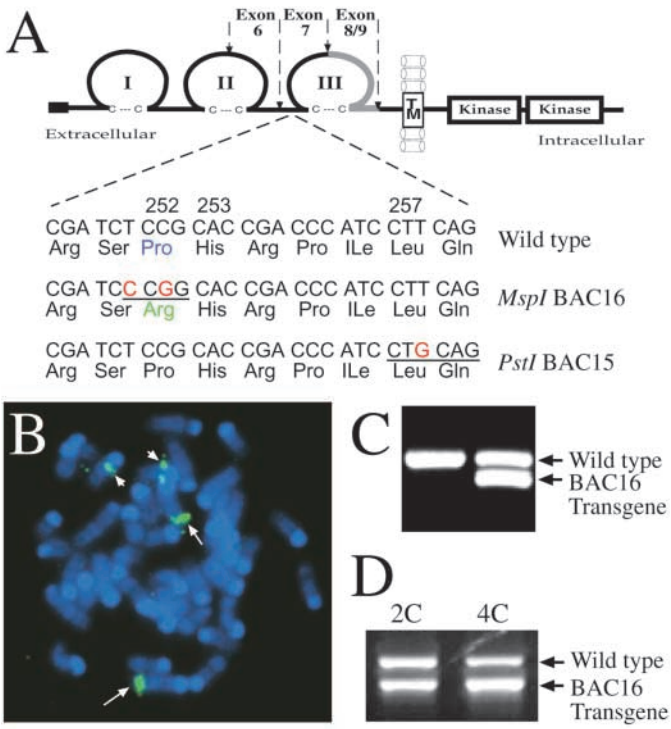

Fig. 1. Generation and analysis of mutant BAC transgenes. (A) Schematic drawing of Fgfr1, harbouring three extracellular immunoglobulin (Ig)-like domains, with relative contributions of exons 6-9 indicated (dashed arrows). The grey region in the C-terminal half of the third Ig loop (III) shows the position of alternative splicing between the IIIb and IIIc isoforms, generated by the use of exons 8 or 9, respectively. Dashed lines expand and highlight the nucleotide sequence of the linker region where the Pro252Arg activating mutation (BAC16) and Leu257Leu silent mutation (BAC15) were introduced by base substitutions. Note that the modifications also introduce *Msp*I-sensitive (BAC16) or *Pst*I-sensitive (BAC15) sites (underlined). (B) FISH analysis, using Fgfr1 probes on metaphase chromosomes, shows integration of BAC transgene into chromosome 4 (arrows). This particular sample was derived from a 4C-transgene animal (see text) and, accordingly, the signal from the transgene is twice as intense as that emanating from the endogenous allele on chromosome 8 (arrowheads). (C) Reverse-transcriptase PCR (RT-PCR) products generated by primers from exons 6 and 8, exposed to *Msp*I enzyme and resolved on a 3% agarose gel. Left and right lanes, products derived from wild-type and BAC16 mouse liver RNA, respectively. Note that the level of transgene expression (303 bp) is equal in intensity to that of the wild-type (343 bp). (D) Resolution of PCR products amplified from tail genomic DNA and digested with *Msp*I. In the left lane (2C), the intensity of the mutant bands is equal to that of the wild type, whereas in the right lane, the mutant band is almost twice as bright. Measurements of these intensities using NIH-imaging software confirm a 2:2 ratio for the 2C, and greater ratios for the 4C mutants (values not shown).

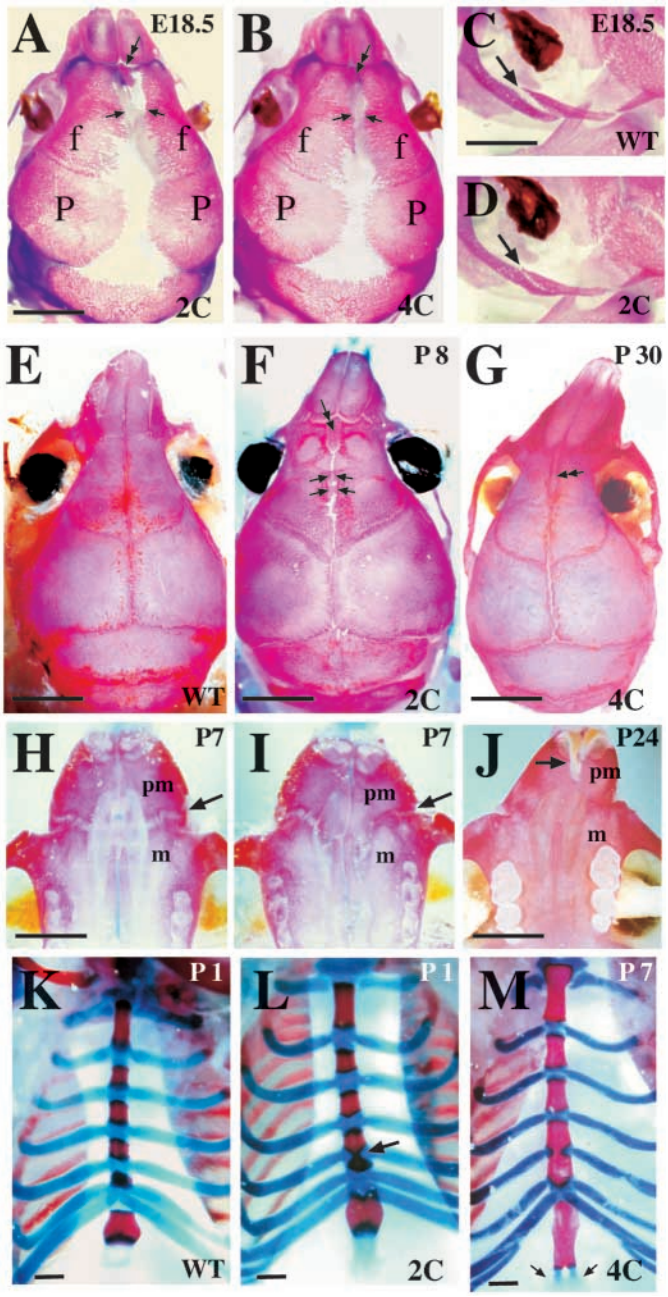

Fig. 2. Cranial and sternal defects in 2C- and 4C-BAC16 mutants. (A,B) Dorsal views of E18.5 skulls, showing presence of boney islands (double arrows) and a more advanced medial growth/ossification of frontal bones (f; distance between arrowheads) in 4C (B) compared with 2C (A) mutants. Apposition of parietal bones (P) also appears to be marginally advanced. (C,D) Lateral view of zygomatic arch bones at the lower rim of the left eye, showing advanced/premature ossification of sutures (arrows) separating the zygomatic branch of maxilla and the jugal bones in a 2C mutant (D) compared with wild type (C). (E-G) Dorsal views of older wild-type (E), 2C (F) and 4C (G) mutant skulls, showing growth and persistence of boney islands (double arrowheads) within the metopic sutures, as well as precocious synostosis of frontal bones (arrows in F). 2C mutant (F) also shows the slight bending of the face that becomes more severe in 4C mutants (G). (H-J) Ventral views of the palate from a wild-type (H), a 2C (I) and a 4C (J) BAC16 mouse. Arrow (I) indicates fusion of the joint separating the left premaxilla (pm) and maxillary (m) bones. Note that the joint on the right is patent. (J) The left pm appears less developed and the incisors have overgrown/ ingrown (arrow). (K-M) Frontal views of the sternum stained for both Alizarin Red and Alcian Blue. (K) Wild type; (L) 2C mutants; (M) 4C mutants. 2C mutant (L) shows fusion of the fourth and fifth sternebrae (arrow) through ectopic ossification of their intervening cartilage. (M) Precocious ossification is more advanced in 4C mutants, and the xiphoid process is also bifurcated (arrows). Scale bars: 1 mm in C,K,L,M; 2mm in A; 2.5 mm in H; 3 mm in F,J; 4 mm in E; 5 mm in G.

embryonic stages did not reveal any evidence for misexpression of the transgene or endogenous *Fgfr1*. Expression of the mutant *Fgfr1* alleles in BAC16 and BAC15 mice by these criteria therefore faithfully recapitulates the behaviour of the endogenous gene in both pattern and levels of expression. The relative ratio, and hence expression of mutant and wild-type receptors, can therefore be incrementally varied by intercrossing mice harbouring two copies of the BAC. Hereafter, the heterozygous BAC16 animals will be termed 2C and the homozygous BAC16 mice will be termed 4C.

Phenotype of 2C-BAC16 mice: defects in endochondral and membranous ossification

We began our analysis by examining the skeletons of BAC15 and 2C-BAC16 mice (Fig. 2; see also Tables S1 and S2 at http://dev.biologists.org/supplemental/). In contrast to sporadic phenotypes seen in BAC15s, which did not correlate with BAC transgene copy number, 2C-BAC16 mutants invariably presented defects in the cranium and the sternum, tissues that develop through two distinct modes of ossification: membranous and endochondral. In the skull, the BAC16 mutation yielded fusion (synostosis) of frontal bones through precocious ossification of the metopic (frontal) sutures. This was apparent as early as embryonic day 18.5 (E18.5) in the form of bony islands (Fig. 2A), but was more obvious at postnatal day 8, when a bony bridge across the metopic sutures linked the two adjacent bones (Fig. 2F). These bridges formed on the dural side of the suture, and it is noteworthy that interactions between sutures and dura mater have been shown to regulate calvarial suture patency (Kim et al., 1998; Opperman et al., 2002). Synostosis of sagittal sutures (separating the parietal bones) and coronal sutures (separating the parietal and frontal bones) was not observed. Further skull defects included shortening of the midface, curved maxilla, and fusion of joints separating the zygomatic arch bones (elements that make up the lower rim of the eye socket), which also develop through membranous ossification. Zygomatic fusion more frequently involved the anterior joint (separating the zygomatic branch of maxilla and the jugal bone) and occurred in a unilateral or bilateral fashion (Fig. 2D). Shortening of the face has been correlated with disparate growth of bones at the base of skull and fusion of their intervening joints (Eswarakumar et al., 2002). We could not detect fusion in joints separating the exoccipital, basi-occipital and basi-sphenoid bones (not shown), but in mice with facial curvature, we found a direct correlation between the phenotype (n=5/5) and unilateral fusion of joints separating the maxilla and pre-maxilla (Fig. 2I,J).

2C-BAC16 mutants also presented sternal defects. The

sternum forms through migration and medial fusion of two lateral-plate-mesoderm derived elements, which undergo endochondral ossification in regions not contacted by ribs, resulting in the formation of six sternebrae separated by cartilage. It has been suggested that rib heads initially inhibit sternal ossification (Chen, 1952; Braun et al., 1992). In 2C-BAC16 mutants, despite the presence of correct rib number and normal articulation of the sternum with ribs, the fourth and fifth sternebrae were fused, suggestive of an over-riding of the inhibition imposed by ribs (Fig. 2L,M).

These observations show that Fgfr1 signalling resulting from expression of the Pro252Arg mutant receptor selectively affects the development of the skeleton, targets distinct bones and sutures, and affects both membranous and endochondral modes of ossification. The range of defects described here are similar to those reported by other studies of hyperactive Fgfr function in mice (Zhou et al., 2000; Hajihosseini et al., 2001; Wang et al., 2001), and to the cranial and skeletal defects observed in Pfeiffer patients (Muenke et al., 1994; Roscioli et al., 2000). In this respect, it should be noted that some phenotypic features of the 2C-BAC16 model, such as sternal fusions, have not previously been described in Pfeiffer patients. However, it is possible that these defects do occur in Pfeiffer syndrome but have not been previously looked for. It should also be noted that the 2C-BAC16 mice, like the model of Zhou et al. (Zhou et al., 2000), did not show defects in the development of the halluces described in Pfeiffer syndrome.

The phenotype of 4C BAC16 mice: limb and axial skeleton defects

A valuable feature of the BAC model employed in these experiments is the ability to manipulate mutant gene copy number and the consequent expression of mutant transcripts. In particular, it is predicted that a doubling of gene copy number by intercrossing 2C-BAC16 mice would further accentuate signalling via mutant receptors, as it favours the formation of mutant receptor homo-dimers, which are required for mutant gene function in the presence of ligand. 2C-BAC16 mice were intercrossed to produce 4C-BAC16 mice (Fig. 1D), which were recovered in the expected Mendelian ratios.

4C-BAC16 mice presented more severe cranial and sternal phenotypes. The curvature of the maxillary process was accentuated (Fig. 2G,J), resulting in mis-aligned jaws and overgrown or in-growing teeth, particularly the incisors. Fusion of zygomatic arch bones was also accentuated, such that in some 4C-mutants both the anterior and posterior joints showed precocious ossification (not shown). This indicates that increasing signalling via mutant Fgfr1 accentuates the severity of the endochondral and membranous bone defects in a quantitative manner.

A key finding, however, was that 4C-BAC16 mice presented a novel set of phenotypes, involving homeotic transformations of the axial skeleton and pre-axial polydactyly of the hind limbs.

Defects in axial patterning

The mouse vertebral column is composed of distinct sets of bones that show unit and segmental identity resulting from the expression of a particular set of Homeobox (Hox) genes (reviewed by Gaunt, 2000). A subset of 4C-BAC16s (*n*=7/15) presented fusion and homeotic transformations of the axial skeleton in a posterior direction. Cervical vertebrae 6 (C6) acquired a C7 identity, and C7 acquired a Thoracic vertebrae 1 (T1) identity (Fig. 3B-D). In one mutant, these transformations were accompanied by fusion of the first and second ribs with an accompanying sternal defect (Fig. 3C). In another, C1 was found to be fused to C2 (not shown). Interestingly though, these defects occurred predominantly in a unilateral fashion, on the left side. In the lower lumbar region of the same animals, L6 often acquired a Sacral (S)1 identity, but this transformation was always bilateral (Fig. 3F). These transformations are similar to those seen in mice carrying a Y766F gain-of-function mutation in *Fgfr1* (Partanen et al., 1998), and in those lacking *caudal-related* genes (Cdx) (Van den Akker et al., 2002).

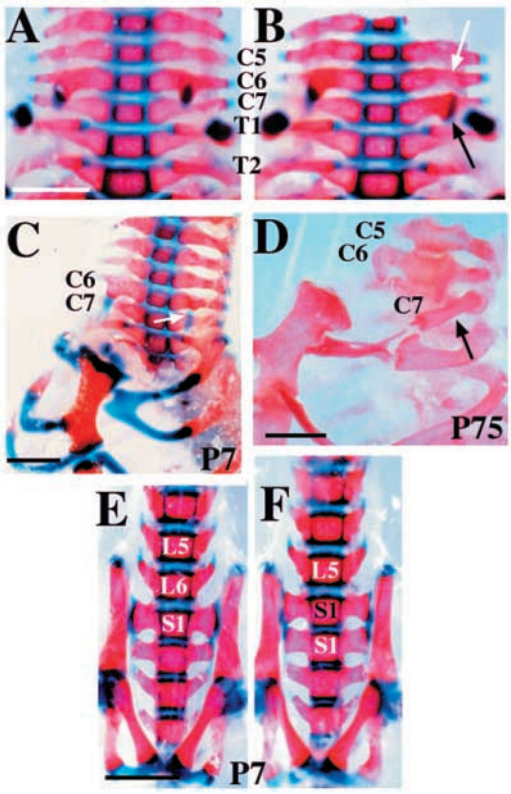

Fig. 3. Homeotic transformations within the vertebral column. (A,B) Ventral views of the cervical and upper thoracic vertebrae from P7 wild-type (A) and a 4C-BAC16 mutant (B) littermates. The clavicle, first sternebrae (manubrium) and ribs have been removed to expose the vertebrae. (B) The left side of the sixth cervical vertebrae, C6, has lost its anterior tuberculum (white arrow), whereas C7 has acquired a rudimentary process (black arrow). (C,D) Left lateral views of the same region in two other 4C animals. (C) Partial loss of C6 anterior tuberculum (white arrow) accompanied by fusion of ribs 1 and 2, and their lack of articulation with the sternum. Note that this lack of articulation results in precocious ossification in the joint separating the manubrium and second sternebrae. (D) The left part of C7 behaves like T1, by extending a rudimentary bone (black arrow) that articulates abnormally with the first rib. (E,F) Ventral views of lower lumbar and upper sacral vertebra of wild-type (E) and 4C-BAC16 (F) littermates. (F) The sixth lumbar vertebrae has acquired an S1 fate and begins to articulate with the adjacent pelvic bones. Scale bars: 2 mm in A,C,D; 3 mm in E,F.

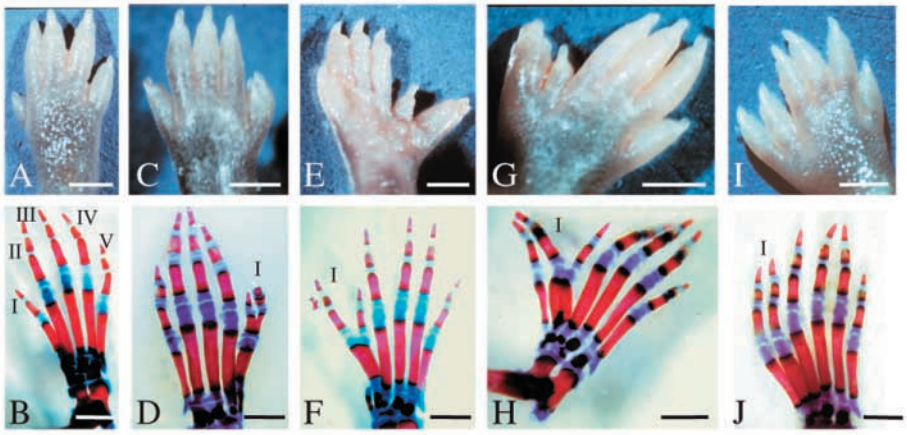

Fig. 4. Range of pre-axial polydactylies observed in the hind limbs of 4C-BAC16 mutants. (A,C,E,G,I) Polydactylous limbs prior to skeletal preparation/staining. (B,D,F,H,J) The corresponding skeletal structure after staining with Alcian Blue and Alizarin Red. (A,B) Dorsal view of postnatal day 6 wild-type right hind limb, showing the biphalangeal nature of digit I (toe) and triphalangeal nature of digits II-V. (C,D,F-J) Dorsal views of postnatal day 7 mutant limbs; (E) ventral view. (C,D) Left hind limb; (E-J) right hind limbs; C-F show limbs from the same animal. Note the triphalangeal nature of mutant digit I in F,H,J. The most frequent form of polydactyly observed (n=7/18) was that shown in F, and in seven out of eight bilateral polydactylous limbs, this type of defect was accompanied by the type shown in D. Note that there is no abnormality in shape, size, length or rate of ossification of the remaining digits. Scale bars: 2 mm in B,D,F,H,I,J; 3 mm in A,C,E,G,I.

Preaxial polydactyly in hindlimbs

A majority of 4C-BAC16 mutants exhibited pre-axial polydactyly. These involved the hindlimbs only, occurring either in a unilateral (9/17 right limb only, 2/17 left limb only) or bilateral fashion (Fig. 4; see Table S2 at http://dev.biologists.org/supplemental/). Within each abnormal limb, only digit I (hallux) was affected, and polydactyly was accompanied by overlying soft tissue syndactyly. Skeletal preparations revealed a range of defects, from a broad toe split at the level of phalanx 1 and 2, to complete duplication of digit I bones and their subsequent transformation into two triphalangeal elements (Fig. 4D-J).

The relationship between mutant gene copy number and limb defect was confirmed by breeding 4C-BAC16 mutants with wild-type mice. The resulting 2C mutant offspring reverted to the milder cranial phenotype, and lacked limb and vertebral defects (n=18, from 3 different breeding pairs).

These results show a direct relationship between mutant Fgfr1 copy number (or ratio to wild-type alleles) and the severity of phenotypes observed. In particular, cranial and sternal development exhibited 'morphogen' characteristics, where the severity of the defect is accentuated by increasing the expression of the mutant gene. However, the development of the axial skeleton and digit I exhibited 'threshold' characteristics, in which the mutant phenotypes only appear when mutant genes are present in excess over their endogenous counterparts.

Candidate gene analysis of polydactyly in 4C-BAC16 hindlimbs

Much is known about genes that control growth and patterning of the vertebrate limbs in the three primary axes (dorsoventral, anteroposterior and proximodistal) (Martin, 1998; Capdevila and Izpisua Belmonte, 2001). Moreover, targeted mutations in mice or spontaneous mutations in man have implicated a number of genes and pathways in pre-axial polydactyly (see Table S3 at http://dev.biologists.org/supplemental/) (Biesecker, 2002). This provided a list of candidate genes that could mediate the threshold-dependent polydactyly phenotype of 4C-BAC 16 mice. We performed a comprehensive analysis of this candidate gene set, comparing expression patterns in wild-type, 2C-BAC16 and 4C-BAC16 limbs by whole-mount in situ hybridisation. For each gene, the analysis focused on embryonic stages previously shown to correspond with either optimal expression and/or a crucial function.

From the candidate gene set listed in Table S3, the majority, including *Shh* (Fig. 5A), exhibited a normal expression pattern in both 2C-BAC16 and 4C-BAC16. However, we did detect alterations in the expression patterns of participants in three pathways: the Hox gene pathway, in the form of the d-cluster Homeobox 13 (*Hoxd13*); the calcium-dependent Wnt pathway, in the form of ligand *Wnt5a*; and the canonical β-catenin Wnt pathway, in the form of *Dickkopf* (*Dkk1*).

In wild-type and 2C-BAC16 E11.0 embryos, expression of *Hoxd13* was restricted to the posterior two-thirds of the distal hind limb buds, covering domains that generate triphalangeal digits II-V. However, in 4C-BAC16 hind limb buds, this expression extended anteriorly to the region that generates digit I (Fig. 5C). Ectopic expression was maintained at E12.5, when the abnormal hind limbs were easily recognisable by the presence of a larger and broader digit I (Fig. 5E).

At E11.5, *Dkk1* is normally expressed throughout the apical ectodermal ridge (AER) and in the hind limbs, strongly in a region that roughly corresponds to parts of the anterior necrotic zone (ANZ) (Fig. 5F,G) (Mukhopadhyay et al., 2001). In eight out of ten 4C-BAC16 hind limbs, the level of *Dkk1* expression was reduced in the anterior two-thirds of the AER, and lost in the ANZ (Fig. 5F,H). Cell death in the developing limbs contributes to the final shape of the autopod, and expression patterns and functional data suggests that Dkk1 has a role in inducing cell death (Grotewold and Ruther, 2002). Thus to examine any potential differences in cell death, we labelled E12.5 embryos with Neutral Red dye, a faithful marker of apoptotic cells in developing limbs (Macias et al., 1996; Hajihosseini and Heath, 2002). In normal and 2C hind limbs, extensive cell death was noted in the mesenchyme anterolateral to the digit I condensate. By contrast, and consistent with the differences in *Dkk1* expression, we found significantly reduced cell death in the corresponding region of 4C abnormal limbs (Fig. 5I).

Wnt5a has been highlighted as a member of the Wnt family that plays a crucial role in distal limb outgrowth, as well as in

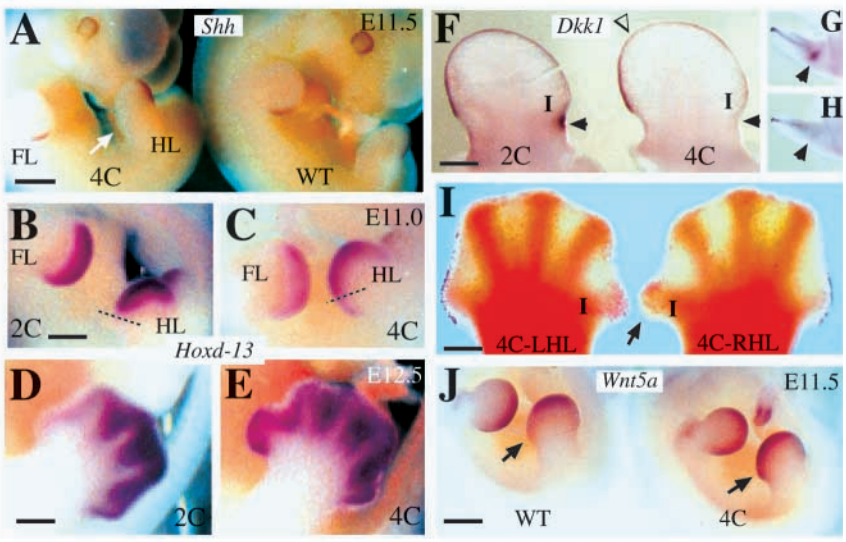

Fig. 5. Gene expression and patterns of cell death in developing 4C-BAC16 limbs. (A) Identical pattern of *Shh* expression in 4C-BAC16 mutant and wild-type limb buds. White arrow indicates the anterior part of mutant hind limb. (B-E) Expression patterns of *Hoxd13* in the right hind limbs of 2C (B,D) and 4C (C,E) BAC16 mutants. 2C-BAC16 expression patterns resemble wild type (not shown). Dashed lines (B,C) represent the expected normal posterior-anterior limit of *Hoxd13* expression in developing hind limb buds; limb anterior is towards the bottom of photograph. (F) Medial and (G,H) anterior views of 2C (G) and 4C (H) E11.5 hind limb buds, showing a reduction in *Dkk1* expression in the anterior two-thirds of the AER (region between the open arrowhead and black arrowhead) in the 4C-BAC16 limb. The 2C pattern resembles wild type (not shown) and 'I' marks the anterior side of each limb corresponding to where digit I develops. Arrowheads point to the ANZ, where *Dkk1* expression is completely quenched in the 4C limb bud. (I) Dorsal view of left and right hind limbs (LHL and RHL) from a 4C-BAC16 mutant stained with Neutral Red. The cell death pattern in this 4C-LHL resembles that of wild type (not shown). 'I' marks the position of developing digit I condensates and the arrow indicates the absence of Neutral Red-positive cells in the abnormal (larger digit I) right hind limb, compared with the presence of such cells in the corresponding region in the normal left hind limb. Also note the similar, unperturbed, patterns of Neutral Red staining at the posterior margins of each limb. (J) Comparison of *Wnt5a* expression in wild-type and 4C-mutant embryos shows a higher *Wnt5a* signal in both fore and hind limbs of 4C-mutants, when compared with the wild type, particularly in the region generating digit I in the hind limb buds (arrows). Scale bars: 400 μm in F,I; 600 μm in B,D; 1.0 mm in J; 1.2 mm in A.

anteroposterior patterning of the early limb bud (Dealy et al., 1993; Parr et al., 1993; Kawakami et al., 1999; Yamaguchi et al., 1999). We thus compared the patterns of *Wnt5a* expression between wild-type, 2C- and 4C-mutant limbs, only to discover a higher intensity of labelling throughout the distal fore and hind limbs of 4C embryos. More relevant to the described limb phenotypes, *Wnt5a* expression was upregulated in the hind limb digit I region of 4C mutants, when compared to 2C mutants or wild-type mice (Fig. 5J).

These results indicate that threshold-dependent hindlimb polydactyly in 4C-BAC16 mice arises through defects in tissue growth and patterning resulting from elevation of mutant receptor signalling. The majority of candidate preaxial polydactyly pathways, such as the Shh or BMP pathway and related genes, appeared unaffected in 4C-BAC16 mutant mice, although we cannot eliminate an increase in the activity of these pathways that does not result in changes in gene expression.

Discussion

We set out to examine the dynamic properties of Fgfr1 signalling pathways in development using the Fgfr1 Pro252Arg mutation, which is predicted from biochemical studies to exhibit quantitatively distinct signalling properties to its wild-type counterpart. We find that the presence of the mutant gene results in some, but not all, of the skeletal defects observed in the equivalent human condition, Pfeiffer syndrome. The phenotypic severity of these defects is enhanced by increasing mutant gene copy number, consistent with a 'morphogen' mode of signalling. However, we also observe the sudden appearance of defects in the development of the axial skeleton and digit I of the hind limb when signalling via the mutant receptors crosses a critical value, defined in these experiments by the ratio of mutant to wild-type gene expression. Fgfr1 therefore exhibits both morphogen and threshold signalling dynamics in the development of the skeleton, depending upon the target pathway employed. These findings indicate that a complete understanding of FGF signalling in development requires not only a definition of the connectivity of signalling pathways across different tissues, but also an understanding of signalling dynamics.

Mechanistic properties of signalling thresholds

Threshold signalling may be contrasted with morphogen signalling, in that in the former there is a 'binary' response to receptor activation whereas in the latter there is a quantitative relationship between receptor occupancy and response, until saturation of receptors by ligand occurs (Freeman and Gurdon, 2002). In both cases, receptor-mediated activation is controlled by the availability of ligand and the affinity of the ligand for the receptor. In pathways that exhibit threshold properties, a covalent modification (e.g. phosphorylation or ubiquitinylation) is usually linked to a process in which the modification is reversed or inhibited (reviewed by Ferrell, 1999; Salazar and Hofer, 2003; Germain, 2001; Germain and Stefnova, 1999). Thus, the difference between the two types of signalling characteristics is explained by the presence of limiting inhibitory pathways in threshold signalling; in morphogen type systems these inhibitory pathways are absent or compromised (Ortega et al., 2002), and there is therefore a direct relationship between receptor occupancy and signal output. The results reported here therefore show that the development of the axial skeleton and digit I of the hind limb involve Fgfr1-mediated signalling pathways that have different regulatory properties from those involved in the sternum and

cranial sutures. This could include different pathway connectivities and/or the presence or absence of inhibitory regulators.

Morphogen signalling in cranial and sternal defects

Mice harbouring 2C-BAC16 alleles exhibit both endochondral and membranous bone defects, including premature fusion of cranial sutures, the zygomatic bones and the sternum. The precocious ossifications and suture fusions reported here are consistent with the proposed role of signalling via Fgfr1 in the induction of osteogenic precursor cell terminal differentiation (Colvin et al., 1996; Iseki et al., 1997; Iseki et al., 1999; Rice et al., 2000; Zhou et al., 2000; Eswarakumar et al., 2002; Huang et al., 2003). These sites of action are similar to those observed in the equivalent mutation in man (Muenke et al., 1994; Roscioli et al., 2000), and in a knock-in mouse model reported by Zhou et al. (Zhou et al., 2000). We were, however, also able to show that the severity of these defects increased when the mutant/wild-type expression ratio is doubled, indicating that osteogenic differentiation is accelerated as signalling via Fgfr1 increases.

The effects of the mutant *Fgfr1* gene in these tissues are restricted to specific bones and sutures. In the skull vault, we observed synostosis of metopic (frontal) but not coronal or sagittal sutures. In the skull base, only the joints separating the maxilla from the pre-maxilla were fused. This differential sensitivity of specific sutures to the presence of mutant receptors could represent sites of selective distribution or concentration of FGF ligands, such that Fgfr1 signalling is limited by ligand availability in susceptible sutures but is in ligand excess in non-susceptible sutures. Although multiple Fgf ligands are expressed in the developing calvarial sutures (Hajihosseni and Heath, 2002), little is known about the distribution or activity state of the corresponding proteins. However, sites of ligand-limited signalling would be susceptible to the experimental addition of extra ligand. Indeed, Iseki et al. and Greenwald et al. have demonstrated that coronal and metoptic sutures undergo premature fusion when exposed to additional Fgf ligand (Iseki et al., 1997; Iseki et al., 1999; Greenwald et al., 2001). Collectively, these findings show that sculpture of the cranium through differential rates of suture fusion in normal development is quantitatively controlled by the availability of Fgf ligand.

Threshold responses in the axial skeleton

4C-BAC16, but not 2C-BAC16, mice exhibit defects in axial patterning whereby distinct vertebrae acquire a more posterior identity. Partanen et al. (Partanen et al., 1998) observed very similar axial transformations, but not polydactyly, by creating a hypermorphic point mutation Y766F in the putative PLCγ/Shb (Cross et al., 2002) docking site in Fgfr1. It is significant that this allele does not give rise to polydactyly, indicating that the underlying threshold-dependent pathways in limb and axial skeleton development are distinct.

The vertebral column is derived from the somites, which are generated sequentially and in a rostrocaudal manner from the paraxial mesoderm. Segmentation of the paraxial mesoderm is believed to be regulated by an oscillator mechanism involving the Notch signalling pathway (reviewed by Holley and Takeda, 2002). *Fgf8* is expressed in a graded manner caudal to the emerging somites, and ligand overexpression studies have led to the proposal that this corresponds to a wave of Fgf signalling that functions to position segmental boundaries by maintaining the pre-somitic mesodermal cells in an uncommitted state (reviewed by Dubrulle and Pourquie, 2002; Dubrulle et al., 2001; Holley and Takeda, 2002). In this model, the establishment of segment identity occurs when Fgf signalling falls below a predetermined threshold. Our findings support this hypothesis, as it would be predicted that, in the presence of a fixed threshold, the ‘wavefront’ of Fgfr1 signalling would extend in a rostral direction in 4C-mutant mice compared with normal counterparts, in turn leading to somites acquiring a more posterior identity (Dubrulle et al., 2001).

Digit I exhibits threshold responses to Fgfr1 signalling

Current models of limb development hold that the individual elements (autopod, zugopod, stylopod) are specified early. One role of Fgfr signalling is then to expand each of the specified fields to their relevant final size and shape, by regulating cell proliferation/survival and the expression of genes that pattern each element (Dudley et al., 2002; Sun et al., 2002). Expression patterns and genetic dissection studies suggest that in the early limb bud, the effects of AER-derived Fgfs on the adjacent mesenchyme are transduced by Fgfr1 (Peters et al., 1992; Partanen et al., 1998; Eswarakumar et al., 2002). The preaxial ploydactyly in hindlimbs, which occurs when hypermorphic BAC transgene copy number is raised to 4C, shows that the development of digit I, but not digits II-V, is dependent on Fgfr1 signalling levels whereby extra digit elements are formed when Fgfr1 signalling is elevated above a threshold, defined here by the ratio of mutant to wild-type receptors. By contrast, mice harbouring a hypomorphic *Fgfr1* allele specifically lack digit I in the hind limb (Partanen et al., 1998). In addition, conditional inactivation of *Fgf8* in hind limbs specifically affects digit I development (Lewandoski et al., 2000). We conclude that digit I exhibits a particular dependency on Fgfr1 signalling – despite uniform expression of *Fgfr1* throughout the early limb bud mesenchyme – and that a role of Fgfr1 signalling is to regulate the size of the pool of cells destined to give rise to digit I. If Fgfr1 signalling is compromised, the digit I precursor pool is reduced leading to the absence of digit I. If, as a result of altered Fgfr1 signalling dynamics, the precursor pool is amplified above a threshold level, the outcome is preaxial polydactyly.

How can the dependency of digit I development on Fgfr1 signalling levels be explained? First, there could be an asymmetric distribution of Fgf ligands within the AER, such that higher levels in the anterior region corresponding to the presumptive digit I trigger a higher level of mutant receptor activation in the adjacent anterior mesenchyme. However, expression pattern studies to date have shown the converse, with ligands such as Fgf4 being restricted to the posterior AER (Bueno et al., 1996). We have previously shown that *Fgf20* is strongly expressed at the anterior and posterior margins of the developing autopod (Hajihosseini and Heath, 2002), but BAC16 mice do not develop digit V polydactyly.

The second, and in our view more likely, explanation is that the development of digit I versus digits II-V is normally governed by two distinct levels of Fgfr1 signalling. This supposes that an increase in size of the digit I precursor pool depends upon Fgfr1 signalling and is terminated when levels

of Fgfr1 signalling fall below a specified threshold. This threshold mechanism does not operate in the development of digits II-V. In 4C-BAC16 mice, Fgfr1 signalling is elevated and fails to fall below the threshold, resulting in the formation of extra digit elements.

Processes that depend on Fgfr1 signalling in the digit I field could include cell proliferation and/or cell death in the surrounding mensenchyme. Polydactyly in many experimental models is accompanied by a reduction in programmed cell death (Chen and Zhao, 1998; Salas-Vidal et al., 2001). We showed that at E12.5, prior to digit outgrowth, significant cell death does indeed normally occur in the mesenchyme around digit I, and that this is quenched in developing limbs of 4C mutants. We also showed that, in the presence of the hypermorphic 4C allele (but not in the 2C mice), *Dkk1* was downregulated close to a region destined to form digit I. *Dkk1* expression is associated with regions of programmed cell death in the limb (Grotewold et al., 1999), ectopic expression of Dkk1 in the limb promotes apoptosis (Grotewold and Ruther, 2002) and *Dkk1* null mice exhibit polydactyly (Mukhopadhyay et al., 2001). Collectively, this evidence indicates that at least part of the mechanism by which Fgfr1 regulates the digit I precursor field is mediated by a threshold-responsive signal that negatively regulates programmed cell death via target genes such as *Dkk1*.

The threshold-sensitive relationship between Fgfr signalling and *Dkk1* expression/cell death may also hold true for the normal development of digits II-V, as later in limb development *Dkk1* becomes downregulated in the growing digits and becomes restricted to inter-digital mesenchyme (Grotewold and Ruther, 2002). However, as 4C-BAC-16 mice do not develop digit II-V syndactyly, it is likely that this threshold-sensitive control is governed by another Fgf receptor. Fgfr2 would be a good candidate, as gain-of-functions mutations in this gene result in post-axial syndactyly in Apert Syndrome.

4C-BAC16 limbs also exhibit an ectopic anterior shift in the domain of *Hoxd13* expression, which is normally restricted to regions that generate the triphalangeal digits II-V. This shift, in addition to the reduced cell death described above, may contribute to the overgrowth in digit I, as mice with loss of Hoxd13 function have significantly shorter digits (Dolle et al., 1993; Bruneau et al., 2001). However, because Hox genes play crucial roles in pattern formation, the most likely consequence of the *Hoxd13* shift is the endowment of a triphalangeal identity to the expanded digit I pool.

As the normal expression pattern of genes such as *Shh*, *dHand* (*Hand2* – Mouse Genome Informatics), *Gli3* and several Bmps is unperturbed in 4C-BAC16 limbs, the ectopic *Hoxd13* may represent a novel connectivity between *Hoxd13* gene expression and elevated Fgfr signalling. This may be mediated by members of the caudal-related homeobox (Cdx) gene family, as Bel-Vialar et al. (Bel-Vialar et al., 2002) have shown that Hox genes exhibit differential sensitivity to Fgf signalling via a Cdx-dependent pathway. In addition, a subset of *Cdx1/Cdx2* compound mutant mice develop digit I polydactyly and show posterior homeotic transformation of several vertebrae, remarkably similar to those described in this report (Fig. 4) (van den Akker et al., 2002). However, we have been unable to detect expression of these genes in either normal or mutant limbs by WMISH.

Developmental significance of signalling dynamics

Our studies of the hypermorphic Pro252Arg allele of Fgfr1 have highlighted the importance of signalling dynamics in skeletogenesis. In particular, we have shown that, for Fgfr1, some system responses to ligands are quantitatively related to ligand availability and others exhibit a binary switch in response as signalling passes a threshold value. We have argued that these different categories of response reflect differing designs of downstream signalling pathways. This enables major changes in the developmental process, either evolutionary or pathological, to be effected by changing the 'values' of the signalling pathways rather than the connectivity.

This work was supported by grants from the Wellcome Trust to J.K.H. and A.O.M.W. M.D.L. was supported in part by an EMBO fellowship. We are very grateful to Karen Faulkner, Celine Jones and Katherine Larkins for their technical help, and Heiner Schrewe for critical reading of the manuscript. We also thank the following for providing plasmids encoding the relevant genes indicated: G. Morris-Kay (Alx4); M. Mallo (Bmps); C.-H. Heldin (BmpR); J. Dechamps (Cdx1 and Cdx2); C. Niehrs (Dkk1); E. Olson (dHand); D. Duboule (Hoxd12 and Hoxd13); A. Zuniga/R. Zeller (Gremlin); R. Hill/A. Compagni (Gli3, Msx1 and Msx2); R. Grosschedl (Lef1); A. Buck (Sall1); J. Chan (Twist); and P. Salinas (Wnt5a).

References

Anderson, J., Burns, H. D., Enriquez-Harris, P., Wilkie, A. O. and Heath, J. K. (1998). Apert syndrome mutations in fibroblast growth factor receptor 2 exhibit increased affinity for FGF ligand. *Hum. Mol. Genet.* **7**, 1475-1483.

Bel-Vialar, S., Itasaki, N. and Krumlauf, R. (2002). Initiating Hox gene expression: in the early chick neural tube differential sensitivity to FGF and RA signalling subdivides the HoxB genes in two distinct groups. *Development* **129**, 5103-5115.

Biesecker, L. G. (2002). Polydactyly: how many disorders and how many genes? *Am. J. Med. Genet.* **112**, 279-283.

Braun, T., Rudnicki, M. A., Arnold, H. H. and Jaenisch, R. (1992). Targeted inactivation of the muscle regulatory gene Myf-5 results in abnormal rib development and perinatal death. *Cell* **71**, 369-382.

Bruneau, S., Johnson, K. R., Yamamoto, M., Kuroiwa, A. and Duboule, D. (2001). The mouse Hoxd13(spdh) mutation, a polyalanine expansion similar to human type II synpolydactyly (SPD), disrupts the function but not the expression of other Hoxd genes. *Dev. Biol.* **237**, 345-353.

Buckle, V. J. and Rack, K. A. (1993). Fluorescent in situ hybridisation. In *Human Genetic Disease Analysis: A Practical Approach*, 2nd edn (ed. K. E. Davies), pp. 59-80. Oxford: IRL Press.

Bueno, D., Skinner, J., Abud, H. and Heath, J. K. (1996). Spatial and temporal relationships between Shh, Fgf4, and Fgf8 gene expression at diverse signalling centres during mouse development. *Dev Dyn* **207**, 291-299.

Capdevila, J. and Izpisua Belmonte, J. C. (2001). Patterning mechanisms controlling vertebrate limb development. *Annu. Rev. Cell Dev. Biol.* **17**, 87-132.

Chen, J. M. (1952). Studies on the morphogenesis of the mouse sternum. *J. Anat. Lond.* **86**, 373-386.

Chen, Y. and Zhao, X. (1998). Shaping limbs by apoptosis. *J. Exp. Zool.* **282**, 691-670.

Chrast, R., Scott, H. S. and Antonarakis, S. E. (1999). Linearization and purification of BAC DNA for the development of transgenic mice. *Transgenic Res.* **8**, 147-150.

Colvin, J. S., Bohne, B. A., Harding, G. W., McEwen, D. G. and Ornitz, D. M. (1996). Skeletal overgrowth and deafness in mice lacking fibroblast growth factor receptor 3. *Nat. Genet.* **12**, 390-397.

Cross, M. J., Lu, L, Magnusson, P., Nyqvist, D., Holmqvist, K., Welsh, M. and Claesson-Welsh, L. (2002). The Shb adaptor protein binds to tyrosine 766 in the FGFR-1 and regulates the Ras/MEK/MAPK pathway via FRS2 phosphorylation in endothelial cells. *Mol. Biol. Cell.* **13**, 2881-2893.

Dealy, C. N., Roth, A., Ferrari, D., Brown, A. M. and Kosher, R. A. (1993). Wnt-5a and Wnt-7a are expressed in the developing chick limb bud in a

manner suggesting roles in pattern formation along the proximodistal and dorsoventral axes. *Mech. Dev.* **43**, 175-186.

Dolle, P., Dierich, A., LeMeur, M., Schimmang, T., Schuhbaur, B., Chambon, P. and Duboule, D. (1993). Disruption of the Hoxd-13 gene induces localized heterochrony leading to mice with neotenic limbs. *Cell* **75**, 431-441.

Dubrulle, J. and Pourquie, O. (2002). From head to tail: links between the segmentation clock and antero-posterior patterning of the embryo. *Curr. Opin. Genet. Dev.* **12**, 519-523.

Dubrulle, J., McGrew, M. J. and Pourquie, O. (2001). FGF signalling controls somite boundary position and regulates segmentation clock control of spatiotemporal Hox gene activation. *Cell* **106**, 219-232.

Dudley, A. T., Ros, M. A. and Tabin, C. J. (2002). A re-examination of proximodistal patterning during vertebrate limb development. *Nature* **418**, 539-544.

Eswarakumar, V. P., Monsonego-Ornan, E., Pines, M., Antonopoulou, I., Morriss-Kay, G. M. and Lonai, P. (2002). The IIIc alternative of Fgfr2 is a positive regulator of bone formation. *Development* **129**, 3783-3793.

Ferrell, J. E. (1999). Building a cellular switch: more lessons from a good egg. *BioEssays* **21**, 866-870.

Freeman, M. and Gurdon, J. B. (2002). Regulatory principles of developmental signalling. *Annu. Rev. Cell Dev. Biol.* **18**, 515-539.

Gaunt, S. J. (2000). Evolutionary shifts of vertebrate structures and Hox expression up and down the axial series of segments: a consideration of possible mechanisms. *Int. J. Dev. Biol.* **44**, 109-117.

Germain, R. N. (2001). The art of the probable: system control in the adaptive immune system. *Science* **293**, 240-245.

Germain, R. N. and Stefanova, I. (1999). The dynamics of T cell receptor signalling: complex orchestration and the key roles of tempo and cooperation. *Annu. Rev. Immunol.* **17**, 467-522.

Greenwald, J. A., Mehrara, B. J., Spector, J. A., Warren, S. M., Fagenholz, P. J., Smith, L. E., Bouletreau, P. J., Crisera, F. E., Ueno, H. and Longaker, M. T. (2001). In vivo modulation of FGF biological activity alters cranial suture fate. *Am. J. Pathol.* **158**, 441-452.

Grotewold, L. and Ruther, U. (2002). The Wnt antagonist Dickkopf-1 is regulated by Bmp signaling and c-Jun and modulates programmed cell death. *EMBO J.* **21**, 966-975.

Grotewold, L., Theil, T. and Ruther, U. (1999). Expression pattern of Dkk-1 during mouse limb development. *Mech. Dev.* **89**, 151-153.

Hajihosseini, M. K. and Heath, J. K. (2002). Expression patterns of fibroblast growth factors-18 and -20 in mouse embryos is suggestive of novel roles in calvarial and limb development. *Mech. Dev.* **113**, 79-83.

Hajihosseini, M. K., Wilson, S., De Moerlooze, L. and Dickson, C. (2001). A splicing switch and gain-of-function mutation in Fgfr2-IIIc hemizygotes causes Apert/Pfeiffer-syndrome-like phenotypes. *Proc. Natl. Acad. Sci. USA* **98**, 3855-3860.

Holley, S. A. and Takeda, H. (2002). Catching a wave: the oscillator and wavefront that create the zebrafish somite. *Semin. Cell Dev. Biol.* **13**, 481-488.

Huang, R., Stolte, D., Kurz, H., Ehehalt, F., Cann, G. M., Stockdale, F. E., Patel, K. and Christ, B. (2003). Ventral axial organs regulate expression of myotomal Fgf-8 that influences rib development. *Dev. Biol.* **255**, 30-47.

Ibrahimi, O. A., Eliseenkova, A. V., Plotnikov, A. N., Yu, K., Ornitz, D. M. and Mohammadi, M. (2001). Structural basis for fibroblast growth factor receptor 2 activation in Apert syndrome. *Proc. Natl. Acad. Sci. USA* **98**, 7182-7187.

Iseki, S., Wilkie, A. O., Heath, J. K., Ishimaru, T., Eto, K. and Morriss-Kay, G. M. (1997). Fgfr2 and osteopontin domains in the developing skull vault are mutually exclusive and can be altered by locally applied FGF2. *Development* **124**, 3375-3384.

Iseki, S., Wilkie, A. O. and Morriss-Kay, G. M. (1999). Fgfr1 and Fgfr2 have distinct differentiation- and proliferation-related roles in the developing mouse skull vault. *Development* **126**, 5611-5620.

Johnson, D. E. and Williams, L. T. (1993). Structural and functional diversity in the FGF receptor multigene family. *Adv. Cancer Res.* **60**, 1-41.

Kawakami, Y., Wada, N., Nishimatsu, S. I., Ishikawa, T., Noji, S. and Nohno, T. (1999). Involvement of Wnt-5a in chondrogenic pattern formation in the chick limb bud. *Dev. Growth Differ.* **41**, 29-40.

Kim, H. J., Rice, D. P., Kettunen, P. J. and Thesleff, I. (1998). FGF-, BMP- and Shh-mediated signalling pathways in the regulation of cranial suture morphogenesis and calvarial bone development. *Development* **125**, 1241-1251.

Lalioti, M. and Heath, J. K. (2001). A new method for generating point mutations in bacterial artificial chromosomes by homologous recombination in Escherichia coli. *Nucl. Acids Res.* **29**, e14.

Lewandoski, M., Sun, X. and Martin, G. R. (2000). Fgf8 signalling from the AER is essential for normal limb development. *Nat. Genet.* **26**, 460-463.

Macias, D., Ganan, Y., Ros, M. A. and Hurle, J. M. (1996). In vivo inhibition of programmed cell death by local administration of FGF-2 and FGF-4 in the interdigital areas of the embryonic chick leg bud. *Anat. Embryol.* **193**, 533-541.

Martin, G. R. (1998). The roles of FGFs in the early development of vertebrate limbs. *Genes Dev.* **12**, 1571-1586.

McLeod, M. J. (1980). Differential staining of cartilage and bone in whole mouse fetuses by alcian blue and alizarin red S. *Teratology* **22**, 299-301.

Muenke, M., Schell, U., Hehr, A., Robin, N. H., Losken, H. W., Schinzel, A., Pulleyn, L. J., Rutland, P., Reardon, W., Malcolm, S. et al. (1994). A common mutation in the fibroblast growth factor receptor 1 gene in Pfeiffer syndrome. *Nat. Genet.* **8**, 269-274.

Mukhopadhyay, M., Shtrom, S., Rodriguez-Esteban, C., Chen, L., Tsukui, T., Gomer, L., Dorward, D. W., Glinka, A., Grinberg, A., Huang, S. P. et al. (2001). Dickkopf1 is required for embryonic head induction and limb morphogenesis in the mouse. *Dev. Cell* **1**, 423-434.

Oldridge, M., Lunt, P. W., Zackai, E. H., McDonald-McGinn, D. M., Muenke, M., Moloney, D. M., Twigg, S. R., Heath, J. K., Howard, T. D., Hoganson, G. et al. (1997). Genotype-phenotype correlation for nucleotide substitutions in the IgII-IgIII linker of FGFR2. *Hum. Mol. Genet.* **6**, 137-143.

Opperman, L. A., Galanis, V., Williams, A. R. and Adab, K. (2002). Transforming growth factor-beta3 (Tgf-beta3) down-regulates Tgf-beta3 receptor type I (Tbetar-I) during rescue of cranial sutures from osseous obliteration. *Orthod. Craniofac. Res.* **5**, 5-16.

Ornitz, D. M. and Itoh, N. (2001). Fibroblast growth factors. *Genome Biol.* **2**, 3005-3012.

Ornitz, D. M. and Marie, P. J. (2002). FGF signalling pathways in endochondral and intramembranous bone development and human genetic disease. *Genes Dev.* **16**, 1446-1465.

Ortega, F., Acerenza, L., Westerhoff, H. V., Mas, F. and Cascante, M. (2002). Product dependence and bifunctionality compromise the ultrasensitivity of signal transduction cascades. *Proc. Natl. Acad. Sci. USA* **99**, 1170-1175.

Osoegawa, K., Tateno, M., Woon, P. Y., Frengen, E., Mammoser, A. G., Catanese, J. J., Hayashizaki, Y. and de Jong, P. J. (2000). Bacterial artificial chromosome libraries for mouse sequencing and functional analysis. *Genome Res.* **10**, 116-128.

Parr, B. A., Shea, M. J., Vassileva, G. and McMahon, A. P. (1993). Mouse Wnt genes exhibit discrete domains of expression in the early embryonic CNS and limb buds. *Development* **119**, 247-261.

Partanen, J., Schwartz, L. and Rossant, J. (1998). Opposite phenotypes of hypomorphic and Y766 phosphorylation site mutations reveal a function for Fgfr1 in anteroposterior patterning of mouse embryos. *Genes Dev.* **12**, 2332-2344.

Passos-Bueno, M. R., Wilcox, W. R., Jabs, E. W., Sertie, A. L., Alonso, L. G. and Kitoh, H. (1999). Clinical spectrum of fibroblast growth factor receptor mutations. *Hum. Mutat.* **14**, 115-125.

Peters, K. G., Werner, S., Chen, G. and Williams, L. T. (1992). Two FGF receptor genes are differentially expressed in epithelial and mesenchymal tissues during limb formation and organogenesis in the mouse. *Development* **114**, 233-243.

Rice, D. P., Aberg, T., Chan, Y., Tang, Z., Kettunen, P. J., Pakarinen, L., Maxson, R. E. and Thesleff, I. (2000). Integration of FGF and TWIST in calvarial bone and suture development. *Development* **127**, 1845-1855.

Roscioli, T., Flanagan, S., Kumar, P., Masel, J., Gattas, M., Hyland, V. J. and Glass, I. A. (2000). Clinical findings in a patient with FGFR1 P252R mutation and comparison with the literature. *Am. J. Med. Genet.* **93**, 22-28.

Salas-Vidal, E., Valencia, C. and Covarrubias, L. (2001). Differential tissue growth and patterns of cell death in mouse limb autopod morphogenesis. *Dev. Dyn.* **220**, 295-306.

Salazar, C. and Hofer, T. (2003). Allosteric regulation of the transcription factor NFAT1 by multiple phosphorylation sites: a mathematical analysis. *J. Mol. Biol.* **327**, 31-45.

Schlessinger, J. (2000). Cell signalling by receptor tyrosine kinases. *Cell* **103**, 211-225.

Sun, X., Mariani, F. V. and Martin, G. R. (2002). Functions of FGF signalling from the apical ectodermal ridge in limb development. *Nature* **418**, 501-508.

Triman, K. L., Davisson, M. T. and Roderick, T. H. (1975). A method for

preparing chromosomes from peripheral blood in the mouse. *Cytogenet. Cell Genet.* **15**, 166-176.

van den Akker, E., Forlani, S., Chawengsaksophak, K., de Graaff, W., Beck, F., Meyer, B. I. and Deschamps, J. (2002). Cdx1 and Cdx2 have overlapping functions in anteroposterior patterning and posterior axis elongation. *Development* **129**, 2181-2193.

Wang, Q., Green, R. P., Zhao, G. and Ornitz, D. M. (2001). Differential regulation of endochondral bone growth and joint development by FGFR1 and FGFR3 tyrosine kinase domains. *Development* **128**, 3867-3876.

Wilkie, A. O. M. and Morriss-Kay, G. M. (2001). Genetics of craniofacial development and malformation. *Nat. Rev. Genet.* **2**, 458-468.

Yamaguchi, T. P., Bradley, A., McMahon, A. P. and Jones, S. (1999). A Wnt5a pathway underlies outgrowth of multiple structures in the vertebrate embryo. *Development* **126**, 1211-1223.

Zhou, Y. X., Xu, X., Chen, L., Li, C., Brodie, S. G. and Deng, C. X. (2000). A Pro250Arg substitution in mouse Fgfr1 causes increased expression of Cbfa1 and premature fusion of calvarial sutures. *Hum. Mol. Genet.* **9**, 2001-2008.

Table S1. Tabulation of skeletal analysis for BAC15 mice

				Craniofacial defects					Sternum	Limbs
Genotype	Code	Age	Sex	Sutures	Bony Isl.	Zygo. Fus.	Face	O.g. Teeth	Fusion	L/R (Type)
Wild type	Tg83-3/3-b.3	P4	n.d.	_	_	_	_	_	_	_
	Tg83-3/3-c.1	P4	n.d.	_	_	_	_	_	_	_
	Tg83-3/3-c.2	P4	n.d.	_	_	_	_	_	_	_
	Tg83-3/6B-a.4	P6	n.d.	_	Y	_	_	_	_	_
	Tg83-3/6B-a.9	P6	n.d.	_	Y	_	_	_	_	_
	Tg83-3/3-a.1	P6	n.d.	_	_	_	_	_	_	_
	Tg83-3/6B-a.9	P6	n.d.	_	Y	_	_	_	_	_
Total = 7										
1C-BAC15	Tg83-3/3-b.1	P4	n.d.	_	_	_	_	_	_	_
	Tg83-3/3-b.2	P4	n.d.	_	_	_	_	_	_	_
	Tg83-3/3-b.5	P4	n.d.	_	_	_	_	_	_	_
	Tg83-3/3-b.7	P4	n.d.	_	_	_	_	_	_	_
	Tg83-3/3-c.4	P4	n.d.	_	_	_	_	_	_	_
	Tg83-3/6B-a.1	P6	n.d.	_	Y	_	_	_	_	_
	Tg83-3/6B-a.2	P6	n.d.	_	Y	_	_	_	_	_
	Tg83-3/6B-a.3	P6	n.d.	_	Y	_	_	_	_	_
	Tg83-3/6B-a.5	P6	n.d.	_	Y (v. small)	_	_	_	_	_
	Tg83-3/6B-a.7	P6	n.d.	_	Y	_	_	_	"Y, rib misaligned"	_
Total = 10										
2C-BAC15	Tg83-3/3-a.2	P6	n.d.	_	_	_	_	_	_	_
	Tg83-3/3-a.3	P6	n.d.	_	_	_	_	_	4+5	_
	Tg83-3/3-a.4	P6	n.d.	_	_	_	_	_	_	_
	Tg83-3/3-b.4	P4	n.d.	_	_	_	_	_	_	_
	Tg83-3/3-b.5	P4	n.d.	_	_	_	_	_	_	_
	Tg83-3/3-c.3	P4	n.d.	_	_	_	_	_	_	_
	Tg83-3/6B-a.6	P6	n.d.	_	Y	_	_	_	"4+5, ribs abnormal"	_
Total = 7										
3C-BAC15	Tg83-3/6B-a.8	P6	n.d.	_	Y	_	_	_	_	_
Total = 1										

Wild Type are litter mates of 2C- and 4C- transgenic mice.
n.d., not determined; –, no phenotype; Y, yes; Bony Isl., bony islands; Zygo. Fus., zygomatic fusion; O.g., over grown teeth; R, right; L, left.
For sternal defects: numbers indicate which sternabrae were fused.
Limb L/R, Hind-limb polydactyly with sides of occurrence indicated as L, left and/or, R, right.
For BAC15 data, 3C-BAC15 is derived from breeding 1C and 2C founders.

Table S2. Tabulation of skeletal analysis for BAC16 mice

				Craniofacial defects					Sternum	Limbs
Genotype	Code	Age	Sex	Sutures	Bony Isl.	Zygo. Fus.	Face	O.g. Teeth	Fusion	L/R (Type)
Wild type	Tg90-3/2A-a.2	P1	n.d.	_	Y	_	_	_	4+5	_
	Tg90-3/8G-b.8	P24	n.d.	Bridged	Y	_	_	_	_	_
	Tg90-3/8G-b.10	P24	n.d.	_	_	_	_	_	_	_
	Tg90-3/8A-a.6	2 months	F	_	_	n.d.	_	_	n.d.	_
Total = 4										
1C-BAC16	Tg90-3/11H.5	E18.5	n.d.	_	Y	_	_	n.a.	_	_
	Tg90-3/8G-b.3	P8	M	Fused	Y	Unilateral	_	_	_	_
	Tg90-3/8G-b.4	P8	F	Bridged	Y	Ant. only	Curv.	_	4+5	_
Total = 3										
2C-BAC16	Tg90-3/11H.2	E18.5	n.d.	_	Y	_	_	n.a.	4+5	_
	Tg90-3/11H.3	E18.5	n.d.	_	Y	_	_	n.a.	4+5	_
	Tg90-3/2A-a.1	P1	n.d.	_	Y	_	_	_	_	_
	Tg90-3/2A-a.3	P1	n.d.	_	_	_	_	_	_	_
	Tg90-3/2A-a.5	P1	n.d.	_	_	_	_	_	_	_
	Tg90-3/2A-a.10	P1	n.d.	_	Y	_	_	_	4+5	_
	Tg90-3/2A-a.11	P1	n.d.	_	Y	_	_	_	_	_
	Tg90-3/2B-b.1	P7	n.d.	Fused	Y	Ant. only	_	_	4+5	_
	Tg90-3/2B-b.5	P7	n.d.	Fused	Y	Ant. only	_	_	4+5	_
	Tg90-3/8G-a.6	P24	n.d.	_	_	_	_	_	_	_
	Tg90-3/8G-a.7	P24	n.d.	Bridged	Y	_	_	_	4+5	_
	Tg90-3/8G-a.9	P24	n.d.	_	_	_	_	_	4+5	_
	Tg90-3/8B-a.5	1.5 months	F	Bridged	_	n.d.	_	Upp. Incisors	n.d.	L+R (I)
	Tg90-3/8A-a.2	2 months	M	Bridged	_	n.d.	_	_	n.d.	R
	Tg90-3/8C-a.2	2 months	M	Bridged	Y	Ant. only	_	_	4+5	Curved
	Tg90-3/3I-a.8	5 months	F	n.d.	_	_	_	_	4+5	R (III)
Total = 15										3
4C-BAC16	Tg90-3/11H.1	E18.5	n.d.	Closer appos.	Y	_	_	n.a.	Extra 5+4+5	R (II)
	Tg90-3/11H.4	E18.5	n.d.	Closer appos.	Y	Ant. only	_	n.a.	4+5	R (I)
	Tg90-3/2B-b.2	P7	n.d.	Fused	Y	Ant. only	Slight Curv; S. Max	_	4+5	R (slight I)
	Tg90-3/2B-b.3	P7	n.d.	Fused	Y	Ant. only	_	_	4+5	L+R (I+III)
	Tg90-3/2B-b.4	P7	n.d.	Bridged	_	Ant.+ post.	_	_	4+5	R (II)
	Tg90-3/2B-b.6	P7	n.d.	Bridged	_	Ant. only	Curv.; S. Max	_	1+2; 4+5	R (IV)
	Tg90-3/8G-a.1	P8	M	Fused	Y	R. ant only/L.both	_	_	4+5	L+R (I+III)
	Tg90-3/8G-a.2	P8	F	Fused	Y	Ant.+ post.	_	_	1+2; 4+5	L+R (I+III)
	Tg90-3/8G-a.5	P24	n.d.	Fused	Y	Ant. only	Curv.	Upp. Incisors	4+5	_
	Tg90-3/8B-a.4	1.5 months	F	Bridged	_	n.d.	Slight Curv.	Upp. Incisors	n.d.	L+R (I+III)
	Tg90-3/4-a.1	2 months	M	Bridged	Y	n.d.	Slight Curv.	Upp. Incisors	4+5	_
	Tg90-3/7A-a.5	2 months	F	Bridged	_	Ant.+ post.	Short Max.	Upp. Incisors	1+2; 3+4+5	L (I)
	Tg90-3/7B-a.1	2 months	M	n.d.	Y	Ant.+ post.	_	Upp. Incisors	1+2; 4+5	L+R (I+III)
	Tg90-3/8A-a.1	2 months	M	Fused	Y	n.d.	Curv. Left	Upp. Incisors	n.d.	L+R
	Tg90-3/8C-a.1	2 months	M	_	Y	Ant.+ post.	Short Max.	Upp. Incisors	4+5	R (I)
	Tg90-3/3D-a.1	2.5 months	M	_	_	Ant. only	_	Upp. Incisors	4+5	L+R (I+II)
	Tg90-3/3D-a.2	2.5 months	M	Fused	_	Ant.+ post.	_	Upp. Incisors	Rib mis 4+5	R (II)
	Tg90-3/2B-c.2	3.5 months	M	n.d.	_	Ant. only	Curv. Left	Upp. Incisors	4+5	L+R (I+III)
	Tg90-3/3D-a.7	4 months	F	Bridged	_	n.d.	Curv. Right	Upp. Incisors	n.d.	n.d.
	Tg90-3/3A-a.4	10 months	F	n.d.	_	Ant. only	Mild Left Curv.	Upp. Incisors	4+5	R (III)
	Tg90-3/7C-a.1	13 months	M	n.d.	Y	Ant. only	Curv.; S. Max	Upp. Incisors	4+5	_
	Tg90-3/7C-a.5	13 months	F	Fused	_	Ant. only	_	_	1+2; 4+5	L (II)
Total = 21										17

Wild type are litter mates of 2C- and 4C-transgenic mice.

n.a., not applicable; n.d., not determined; –, no phenotype; Y, yes; Bony Isl., bony islands; Zygo. Fus., zygomatic fusion; Ant., anterior; post., posterior; R, right; L, left; O.g., over grown teeth; Upp., upper.

For facial defects: Curv., curved (with side indicated); S. Max., short maxilla.

For sternal defects: numbers indicate which sternabrae were fused; Rib mis., rib misalignment (as in Fig. 4C).

Limb L/R, Hind-limb polydactyly with sides of occurrence indicated as L, left and/or, R, right.

The type/combinations of polydactyly observed are indicated by symbols I to IV. Each type, I, II, III and IV, is depicted in Fig. 5, in parts F, D, H, and J, respectively.

Table S3. Candidate genes governing limb development and polydactyly

Gene	E10-E10.5	E11-E11.5	E12-E12.5
Alx4	+		
Bmp2		+	
Bmp4	+	+	
BmpRI-B		+	
Cdx1	–	–	
CdX2	–	–	
Dkk1		+	+
Fgf4	+	+	+
Fgf8	+		
Fgfr1	+		
Gli3	+	+	
Gremlin		+	
dHAND	+	+	
Hoxd12		+	
Hoxd13		+	+
Lmbr1	–	–	
Lef1		+	
Msx1		+	
Msx2		+	
Sall1	+		
Shh	+	+	
Twist	+	+	
Wnt5a		+	

List of genes whose expression was examined in wild-type, 2C- and 4C-BAC16 embryonic mice in this study. Studies of engineered or spontaneous mutations (Biesecker, 2002) have implicated a subset of such genes in polydactyly.

+, embryonic stages examined where expression was detected.

–, stages examined where no expression was detected.

Blanks represent stages that were not studied.

A minimum of two embryos were examined at each stage indicated.